

# Topological superconductor from superconducting topological surface states and fault-tolerant quantum computing

Xi Luo<sup>1,\*</sup>, Yu-Ge Chen<sup>2,3,4,\*</sup>, Ziqiang Wang<sup>5,†</sup> and Yue Yu<sup>2,3,4‡</sup>

1. College of Science, University of Shanghai for Science and Technology, Shanghai 200093, PR China

2. State Key Laboratory of Surface Physics, Fudan University, Shanghai 200433, China

3. Center for Field Theory and Particle Physics, Department of Physics, Fudan University, Shanghai 200433, China

4. Collaborative Innovation Center of Advanced Microstructures, Nanjing 210093, China

5. Department of Physics, Boston College, Chestnut Hill, MA 02467, USA

(Dated: March 27, 2020)

The chiral  $p$ -wave superconductor/superfluid in two dimensions (2D) is the simplest and most robust system for topological quantum computation [1, 2]. Candidates for such topological superconductors/superfluids in nature are very rare. A widely believed chiral  $p$ -wave superfluid is the Moore-Read state in the  $\nu = \frac{5}{2}$  fractional quantum Hall effect [3, 4], although experimental evidence are not yet conclusive [5]. Experimental realizations of chiral  $p$ -wave superconductors using quantum anomalous Hall insulator-superconductor hybrid structures have been controversial [7, 8]. Here we report a new mechanism for realizing 2D chiral  $p$ -wave superconductors on the surface of 3D  $s$ -wave superconductors that have a topological band structure and support superconducting topological surface states (SC-TSS), such as the iron-based superconductor Fe(Te,Se) [9]. We find that tunneling and pairing between the SC-TSS on the top and bottom surfaces in a thin film or between two opposing surfaces of two such superconductors can produce an emergent 2D time-reversal symmetry breaking chiral topological superconductor. The topologically protected anyonic vortices with Majorana zero modes as well as the chiral Majorana fermion edge modes ( $\chi$ MEMs) can be used as a platform for more advantageous non-abelian braiding operations. We propose a novel device for the CNOT gate with six  $\chi$ MEMs, which paves the way for fault-tolerant universal quantum computing.

The electronic structure of a large class of the crystalline materials is characterized by a topological  $Z_2$  invariant. Three dimensional (3D) strong topological insulators have a nontrivial  $Z_2$  invariant band structure and support helical Dirac fermion topological surface states (TSS) protected by time-reversal symmetry. Several iron-based superconductors, highlighted by Fe(Te,Se), have emerged recently as charge transfer metals [10] with nontrivial topological  $Z_2$  invariant band structures originating from the  $p$ - $d$  band inversion and spin-orbit coupling (SOC) [11–13]. In the normal state, these Fe-chalcogenides and pnictides have a small Fermi energy and can be considered as topological metals with lightly doped TSS, which have been observed by spin-polarized angle-resolved photoemission spectroscopy (ARPES) [9, 14]. In the fully gapped superconducting (SC) state below  $T_c$ , ARPES shows that the TSS develop a SC gap, induced by bulk superconductivity, comparable to the bulk gap [9]. These remarkably discoveries suggest that superconductors bearing a topological nontrivial  $Z_2$  invariant electronic structure can support a new form of quantum matter on their surfaces – the SC topological surface states (SC-TSS).

The SC-TSS has provided a new platform for finding

Majorana zero modes (MZMs) since the  $\pi$ -Berry phase of the Dirac fermions makes the vortex core states [15] of the SC-TSS carry integer total angular-momentum quantum numbers and naturally support the zero energy mode [16]. Indeed, the SC-TSS is a single-material realization of the Fu-Kane proposal for inducing superconductivity in the TSS of a strong topological insulator by proximity effect to an  $s$ -wave superconductor [17]. Candidate MZMs have been observed as zero-energy bound states inside external magnetic field induced vortices in FeTe<sub>0.55</sub>Se<sub>0.45</sub> [18, 19], (Li<sub>0.84</sub>Fe<sub>0.16</sub>)OHFeSe [20], CaKFe<sub>4</sub>As<sub>4</sub> [21], and quantum anomalous vortices [16] nucleated at the interstitial and adatom magnetic Fe sites in FeTe<sub>0.55</sub>Se<sub>0.45</sub> [22, 23] and LiFeAs [24] without applying an external magnetic field. We report in this article that the SC-TSS can be used to produce an emergent nonmagnetic 2D time-reversal symmetry breaking chiral topological superconductor ( $\chi$ TSC). The necessary ingredient is the coupling of the SC-TSS on the top and bottom surfaces in a thin film (Fig. 1(a)) or between two opposing surfaces of two superconductors (Fig. 1(b)). Such  $\chi$ TSCs provide topologically protected anyonic vortices with MZMs as well as chiral Majorana fermion edge modes ( $\chi$ MEMs) for nonabelian braiding operations. As an example, a CNOT gate device, to be discussed in detail later, is shown in Fig. 1(c) using thin films (blue) hosting six  $\chi$ MEMs for universal quantum computing.

In the Nambu basis, the electron operator  $\Psi_N = (\psi_{1\uparrow\mathbf{q}}, \psi_{1\downarrow\mathbf{q}}, \psi_{2\uparrow\mathbf{q}}, \psi_{2\downarrow\mathbf{q}}, -\psi_{1\downarrow-\mathbf{q}}^\dagger, \psi_{1\uparrow-\mathbf{q}}^\dagger, \psi_{2\downarrow-\mathbf{q}}^\dagger, -\psi_{2\uparrow-\mathbf{q}}^\dagger)^T$ , where 1 and 2 label the surface and  $\uparrow$  and  $\downarrow$  the pseu-

\*These two authors contribute equally.

†Correspondence to: wangzi@bc.edu

‡Correspondence to: yuyue@fudan.edu.cn

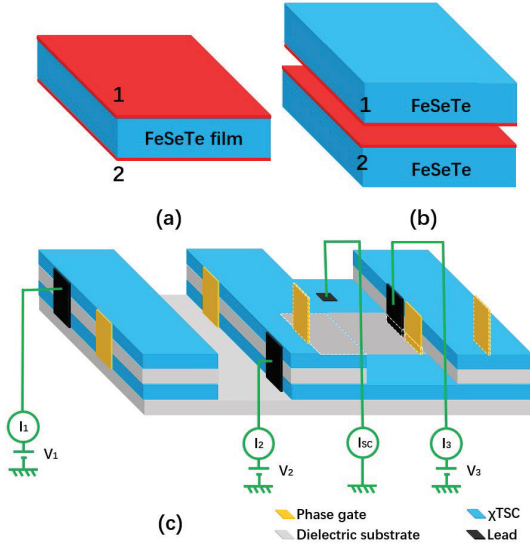


FIG. 1: (color online) The coupled SC-TSS illustrated with FeTeSe. (a) Thin film with top (1) and bottom (2) SC-TSS. (b) Opposing surfaces (1 and 2) of two superconductors with SC-TSS. (c) Schematics of a device for the CNOT gate.

dospin states in the presence of SOC. The system is described by  $H = \frac{1}{2} \sum_{\mathbf{q}} \Psi_N^\dagger h(\mathbf{q}) \Psi_N$ , with the  $8 \times 8$  Bogoliubov-de Gennes (BdG) Hamiltonian matrix

$$h(\mathbf{q}) = h_0(\mathbf{q}) - t\sigma_0\chi_x\tau_0 + h_{12}^\Delta \quad (1)$$

$$h_0(\mathbf{q}) = v_F \mathbf{q} \cdot \boldsymbol{\sigma} \chi_z \tau_z - \mu \sigma_0 \chi_0 \tau_z + \Delta \sigma_0 \chi_0 \tau_x, \quad (2)$$

where  $(\boldsymbol{\sigma}, \sigma_0)$   $(\boldsymbol{\chi}, \chi_0)$ , and  $(\boldsymbol{\tau}, \tau_0)$  are Pauli and unit matrices acting in the pseudospin, surface, and particle-hole sectors, respectively.  $h_0(\mathbf{q})$  in Eq. (2) describes the uncoupled SC-TSS, where  $v_F$  is the Fermi velocity to be set to unity,  $\mathbf{q}$  is the 2D momentum  $(q_x, q_y)$ ,  $\mu$  is the chemical potential, and the real  $\Delta$  is the intra-surface  $s$ -wave pairing strength.  $h_0$  has inversion and particle-hole symmetries, namely,  $\mathcal{P}h_0(-\mathbf{q})\mathcal{P}^{-1} = h_0(\mathbf{q})$  and  $\mathcal{C}h_0(-\mathbf{q})\mathcal{C}^{-1} = -h_0(\mathbf{q})$  with  $\mathcal{P} = \sigma_0\chi_x\tau_z$  and  $\mathcal{C} = \sigma_x\chi_y\tau_y\mathcal{K}$ , respectively, where  $\mathcal{K}$  is the complex conjugation operator. The time-reversal (TR) operation under  $\mathcal{T} = i\sigma_y\chi_0\tau_0\mathcal{K}$  is also a symmetry of  $h_0$  since  $\mathcal{T}h_0(-\mathbf{q})\mathcal{T}^{-1} = h_0(\mathbf{q})$ . Clearly,  $\mathcal{P}^2 = 1$ ,  $\mathcal{C}^2 = 1$ , and  $\mathcal{T}^2 = -1$ .

The couplings between the two surfaces are described by the single-particle tunneling  $t$  and inter-surface pairing  $h_{12}^\Delta$  in Eq. (1). We consider both spin singlet (surface triplet) and triplet (surface singlet) local pairing with real amplitudes,

$$\begin{aligned} H_{12}^{\Delta_s} &= \sum_{\mathbf{q}} \Delta_s (\psi_{1\uparrow\mathbf{q}}^\dagger \psi_{2\downarrow-\mathbf{q}}^\dagger - \psi_{1\downarrow\mathbf{q}}^\dagger \psi_{2\uparrow-\mathbf{q}}^\dagger) + h.c., \\ H_{12}^{\Delta_t} &= \sum_{\mathbf{q}} \Delta_t (\psi_{1\uparrow\mathbf{q}}^\dagger \psi_{2\downarrow-\mathbf{q}}^\dagger + \psi_{1\downarrow\mathbf{q}}^\dagger \psi_{2\uparrow-\mathbf{q}}^\dagger) + h.c., \\ H_{12}^{\Delta_\sigma} &= \sum_{\mathbf{q}} \Delta_\sigma \psi_{1\sigma\mathbf{q}}^\dagger \psi_{2\sigma-\mathbf{q}}^\dagger + h.c. \end{aligned} \quad (3)$$

The spin-singlet pairing  $H_{12}^{\Delta_s}$  is TR invariant (even un-

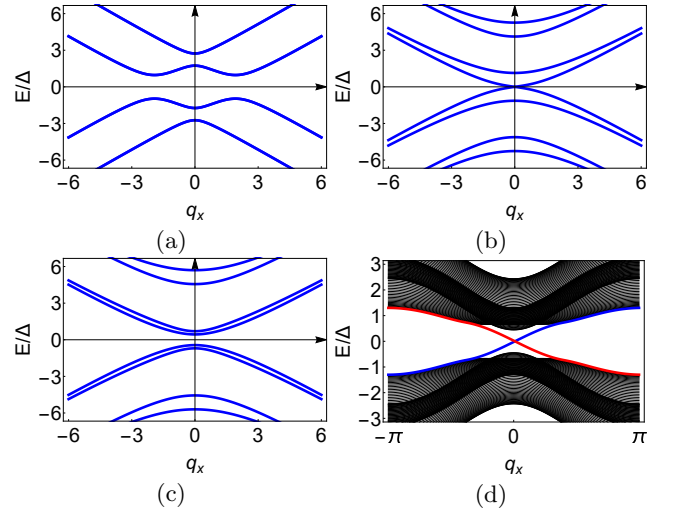


FIG. 2: (color online) Energy spectrum evolution of BdG Hamiltonian  $h(\mathbf{q})$  in Eq. (1), plotted in the  $q_y = 0$  plane for  $\Delta = 1$ ,  $\mu = 2$ , and  $\Delta_s = 0$ . (a)  $t = 0.5$ ,  $\Delta_t = 0$ . (b)  $t = 2.06$ ,  $\Delta_t = 1.5$ . (c)  $t = 2.5$ ,  $\Delta_t = 1.5$ . (d) Energy spectrum of the lattice model with same parameters as in (c) under open boundary condition in  $y$ -direction (50 sites). The red and blue curves are the gapless edge states of a single  $\chi$ MEM.

der  $\mathcal{T}$ ). In contrast, the one-dimensional representation of the spin-triplet pairing,  $H_{12}^{\Delta_t}$  breaks the TR symmetry (odd under  $\mathcal{T}$ ). Similarly, for the two-dimensional equal-spin triplet pairing, the independent basis functions  $H_{12}^{\Delta_t^\uparrow} \pm H_{12}^{\Delta_t^\downarrow}$  are odd and even under  $\mathcal{T}$  respectively [26]. These inter-surface pairings of the SC-TSS bear a formal analogy to the interorbital pairing considered for bulk  $\text{Cu}_x\text{Bi}_2\text{Se}_3$  [25, 27], where purely imaginary spin-triplet  $\Delta_t$  pairing was argued to produce a class DIII TR invariant TSC in 3D [28–30]. For simplicity, we will not consider the equal-spin pairing channels further, since they do not introduce new physics. Thus we have,

$$h_{12}^\Delta = -\Delta_s \sigma_0 \chi_y \tau_y + \Delta_t \sigma_z \chi_x \tau_x, \quad (4)$$

in  $h(\mathbf{q})$  of Eq. (1). The coupling of the SC-TSS by the tunneling and pairing terms ensures the breaking of TR symmetry by a novel nonmagnetic mechanism (see the SI [31] for more detailed symmetry analysis) and the emergence of a chiral superconductor.

To illustrate the intrinsic  $\mathcal{T}$ -breaking phase induced by  $\Delta_t$ , we obtain the evolution of the energy spectrum (Fig. 2) of the BdG Hamiltonian for  $\Delta_s = 0$ . The effect of a nonzero  $\Delta_s$  will be discussed later. The values of  $\mu$  and  $\Delta$  are chosen in the range of the known experimental data for  $\text{Fe}_{1+y}\text{Se}_x\text{Te}_{1-x}$  with  $\Delta/\mu = 0.5$  and  $\Delta \sim 2\text{meV}$  [18, 32] which is set to unity. We begin with the case  $\Delta_t = 0$  shown in Fig. 2a, where the intra-surface  $s$ -wave pairing  $\Delta$  opens a SC energy gap and the inter-surface tunneling  $t$ -term further gaps out the two Dirac points separated by  $2\mu$ . Each band in Fig. 2a is doubly degenerate. Turning on  $\Delta_t \neq 0$ , the degeneracy is lifted due to the broken TR symmetry. Increasing  $t$  or  $\Delta_t$  leads to

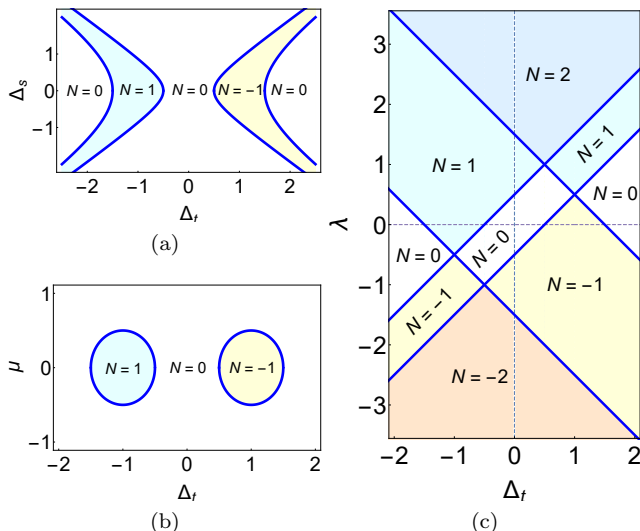


FIG. 3: (color online) Topological phase diagrams in (a)  $\Delta_t$ - $\Delta_s$  plane for  $\mu = 0$ , (b)  $\Delta_t - \mu$  plane for  $\Delta_s = 0$ , and (c)  $\Delta_t$ - $\lambda$  plane for  $\mu = 0$  and  $\Delta_s = 0$ . In (a)-(c),  $t = 0.5$ ,  $N$  is the total Chern number, and blue lines are the phase boundaries.

a gap closing at  $\Gamma$  point (Fig. 2b). The gap then reopens with a band inversion (Fig. 2c) triggering a topological phase transition into the emergent  $\chi$ TSC that supports a single gapless Majorana edge mode localized at the open boundaries (Fig. 2d). This is confirmed by a lattice model study [31], and is consistent with a bulk Chern number  $N = 1$ . Increasing the tunneling  $t$  can cause the gap to close again and the system to return to a topologically trivial superconductor (not shown).

To determine the topological phase structure, we numerically calculate the Berry phase of each band. The topological property of the system is characterized by the total Chern number, i.e. the summation of the Berry phases of the lower four quasihole bands [33]. The regions marked by Chern number  $N = \pm 1$  on the topological phase diagrams in the  $\Delta_t$ - $\Delta_s$  plane at  $\mu = 0$  (Fig. 3a) and in the  $\Delta_t$ - $\mu$  plane at  $\Delta_s = 0$  (Fig. 3b) correspond to the  $\chi$ TSC supporting a single  $\chi$ MEM at the boundaries.

The phase structures (Figs. 3a and 3b) indicate that the  $\chi$ TSC is most prominent in the region of small  $\mu$  and  $\Delta_s$ . It is therefore instructive to explore the nature of the topological phases and phase transitions in the limit of  $\mu, \Delta_s = 0$ . In this case, the solution of the BdG Hamiltonian  $h$  in Eq. (1) can be obtained analytically, even in the presence of an additional TR symmetry breaking Zeeman coupling  $h^\lambda = \lambda \sigma_z \chi_0 \tau_0$ , giving rise to 8 quasiparticle/quasihole bands

$$E_{\mu, \Delta_s=0} = \pm \sqrt{M_a^2 + q^2}, \quad (5)$$

where  $a = 1, \dots, 4$  and  $M_1 = \Delta_t - \lambda + \Delta + t$ ,  $M_2 = \Delta_t + \lambda + \Delta - t$ ,  $M_3 = \Delta_t + \lambda - \Delta + t$ , and  $M_4 = \Delta_t - \lambda - \Delta - t$ . Thus, there is an emergent Lorentz invariance in this limit, as all the BdG bands become relativistic with the corresponding effective mass  $M_a$ . The Chern numbers

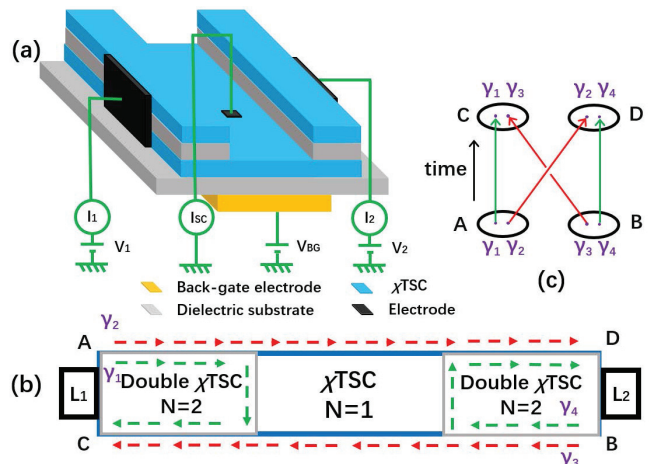


FIG. 4: (color online) (a) A schematic of a layered  $\chi$ TSC structure for nonabelian braiding. The  $N = 2$  phase is achieved by the  $\chi$ TSC-insulator- $\chi$ TSC structure at the two ends. (b) The top view of the device in (a). The arrows stand for the  $\chi$ MEMs which are labeled by  $\gamma_i$ . (c) The electron at the leads splits into two  $\chi$ MEMs and becomes a nonlocal fermion. Under the braiding of  $\gamma_2$  and  $\gamma_3$ , the evolution of the odd parity electron state from terminals A and B to C and D is equivalent to a Hadamard gate followed by a Pauli-Z gate.

associated with the four quasihole bands are,  $\frac{1}{2}\text{sgn}(M_1)$ ,  $-\frac{1}{2}\text{sgn}(M_2)$ ,  $-\frac{1}{2}\text{sgn}(M_3)$ , and  $\frac{1}{2}\text{sgn}(M_4)$ , respectively. Whenever there is a sign change in  $M_a$ , i.e., a band inversion, the total Chern number changes by one. These sign changes as the Zeeman coupling  $\lambda$  and  $\Delta_t$  are varied determine the topological phase diagram in the  $\Delta_t$ - $\lambda$  plane (Fig. 3c). The phases with the total Chern number  $N = \pm 1$  are indeed the  $p$ -wave  $\chi$ TSC [4]. To see this, consider, e.g. the phase with  $\lambda = 0$ ,  $t > \Delta > 0$ , and  $-\Delta - t < \Delta_t < -t$ . The effective BdG Hamiltonian for the two bands closest to zero energy is given by

$$h = \begin{pmatrix} -M_1 & q_x - iq_y \\ q_x + iq_y & M_1 \end{pmatrix}, \quad (6)$$

which is identical to that of a  $q_x + iq_y$ -wave  $\chi$ TCS with an effective chemical potential  $M_1 > 0$ .

Note that the phases along the  $\Delta_t = 0$  line in Fig. 3c are consistent with those proposed in the quantum anomalous Hall insulator (QAHI)-SC proximity hybrid structures [6, 7, 34], where ferromagnetism (thus  $\lambda$ ) is crucial for breaking the TR symmetry. In contrast, along the  $\lambda = 0$  line in Fig. 3c, the TR symmetry is broken by the inter-surface spin-triplet pairing of the SC-TSS, which is nonmagnetic and produces the  $N = \pm 1$  *intrinsic*  $p$ -wave  $\chi$ TSC with a single  $\chi$ MEM. The half-integer quantized conductance  $\frac{e^2}{2h}$  of the  $\chi$ MEM can be detected directly at the edge of an antidot, as discussed in the SI [31].

We turn to TQC using the  $\chi$ MEMs in such  $\chi$ TSCs. A protocol for nonabelian braiding based on the  $\chi$ MEMs has been proposed using the QAHI-(SC+QAHI)-QAHI

proximity structures [35]. In the QAHI, the chiral fermion edge state can be viewed as two  $\chi$ MEMs; one of them propagates to the other side through the edge of the hybrid TSC (SC+QAHI) in the middle region, while the other cannot. Therefore, ideally, the junction braids the  $\chi$ MEMs and forms a nonabelian gate, which is equivalent to a Hadamard gate followed by a Pauli-Z gate [35]. However, the nonabelian braiding in such a system may fail because the SC+QAHI hybrid structure may end up in a metallic phase instead of the desired TSC [36]. Furthermore, there can be vortices in the superconductor, trapping MZMs and change the results of braiding dramatically [37, 38]. These obstacles can be avoided by using the  $\chi$ TSCs. In order to realize the 2D spinor braiding statistics, four Majorana fermions are needed, which form an  $SO(4)$  nonabelian group for the statistics [39, 40]. We therefore construct a novel device with a common thin film  $\chi$ TSC shared by two layered  $\chi$ TSC-insulator- $\chi$ TSC mesas on the sides (Fig. 4a). Each mesa has a Chern number  $N = 2$  and supports two  $\chi$ MEMs on the edges of the top and bottom  $\chi$ TSCs, respectively (Fig. 4b). For an electron in the leads with energy within the SC gap, there are two channels for transport: to enter the bulk  $\chi$ TSC by Andreev reflection or to split into two  $\chi$ MEMs and propagate along the edges. Once Andreev reflection is suppressed, the only open channel is through the  $\chi$ MEMs (Fig. 4b) by splitting the electron into a nonlocal fermion. This can be achieved via single electron tunneling controlled by a gate-induced barrier at the contacts between the leads and the  $\chi$ TSC.

In the low current limit, the incoming electron states at terminals A and B can be represented by the four spatially separated Majorana fermions (Fig. 4b):  $|n_A^{\gamma_1\gamma_2} n_B^{\gamma_3\gamma_4}\rangle$  where  $n_{A,B}$  are the fermion parities. For example,  $|1_A\rangle = \psi_A^\dagger |0\rangle$  with  $\psi_A = \gamma_1 + i\gamma_2$ . The outgoing states at terminals C and D are, similarly, given by  $|n_C^{\gamma_1\gamma_3} n_D^{\gamma_2\gamma_4}\rangle$ . The dimension of the state space for a fixed fermion parity is two, which corresponds to a qubit. Under a braiding operation  $\gamma_2 \rightarrow \gamma_3, \gamma_3 \rightarrow -\gamma_2$ , the evolution of the parity odd electron state is thus equivalent to a Hadamard- followed by a Pauli-Z gate (Fig. 4c)

$$\begin{pmatrix} |0_C^{\gamma_1\gamma_3} 1_D^{\gamma_2\gamma_4}\rangle \\ |1_C^{\gamma_1\gamma_3} 0_D^{\gamma_2\gamma_4}\rangle \end{pmatrix} = \frac{1}{\sqrt{2}} \begin{pmatrix} 1 & 1 \\ -1 & 1 \end{pmatrix} \begin{pmatrix} |0_A^{\gamma_1\gamma_2} 1_B^{\gamma_3\gamma_4}\rangle \\ |1_A^{\gamma_1\gamma_2} 0_B^{\gamma_3\gamma_4}\rangle \end{pmatrix}. \quad (7)$$

To achieve universal quantum computing, we design a CNOT gate between 2-qubits using six  $\chi$ MEMs  $\gamma_1, \dots, \gamma_6$  [41, 42]. The device is shown in Fig. 1c and its top view in Fig. 5a. In the basis of even total fermion parity sector, i.e.,  $(|0_A 0_B 0_C\rangle, |0_A 1_B 1_C\rangle, |1_A 0_B 1_C\rangle, |1_A 1_B 0_C\rangle)^T$ , the counter-clockwise braiding matrices  $R_{ij}$  between the  $\gamma$ 's are  $R_{12} = \text{diag}(1, 1, -i, -i)$ ,  $R_{34} = \text{diag}(1, -i, 1, -i)$ ,  $R_{56} = \text{diag}(1, -i, -i, 1)$ , and

$$R_{23} = \frac{1}{\sqrt{2}} \begin{pmatrix} 1 & 0 & 0 & 1 \\ 0 & 1 & 1 & 0 \\ 0 & -1 & 1 & 0 \\ -1 & 0 & 0 & 1 \end{pmatrix}, R_{45} = \frac{1}{\sqrt{2}} \begin{pmatrix} 1 & 1 & 0 & 0 \\ -1 & 1 & 0 & 0 \\ 0 & 0 & 1 & 1 \\ 0 & 0 & -1 & 1 \end{pmatrix}$$

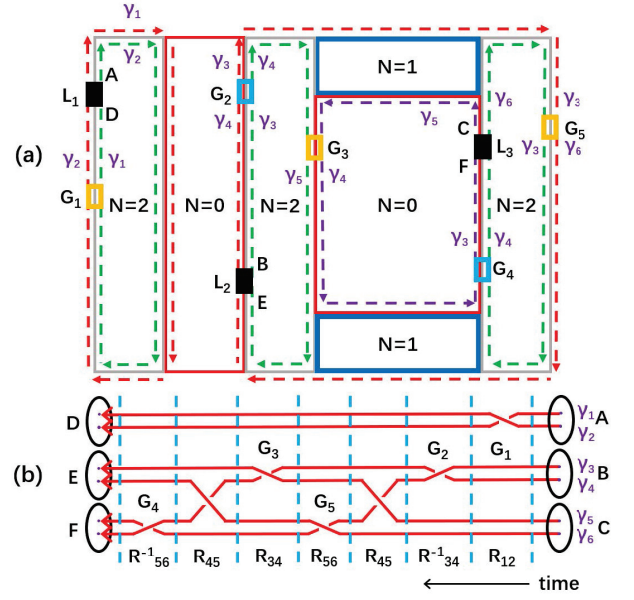


FIG. 5: (color online) (a) The top view of the device for the CNOT gate in Fig. 1c. The substrate is a trivial insulator. A  $\chi$ TSC layer with  $N = 1$  covers the substrate except for the  $N = 0$  region. The  $N = 2$  region is the  $\chi$ TSC-insulator- $\chi$ TSC mesa structure (see Fig. 1c and Fig. 4). The solid black rectangles are the leads while the hollowed ones are the phase gates. For the CNOT gate in the even fermion parity sector, the gate-voltage induced phase shift is  $\theta = \frac{\pi}{2}$  for  $G_1, G_3$ , and  $G_5$ , and  $\theta = -\frac{\pi}{2}$  for  $G_2$  and  $G_4$ . (b) The braiding diagram for the CNOT gate. The dashed blue lines stand for time slices. The braiding  $R$ -matrices are explained in the text.

where the subscripts stand for the relative positions of the  $\gamma$ 's at a given time slice (dashed blue lines in Fig. 5b).  $R_{12}$ ,  $R_{34}$ , and  $R_{56}$  can be realized by tuning the corresponding gate voltages  $V$  over a length  $L$ , e.g.,  $G^{ij}(\theta = VL)|1^{\gamma_i\gamma_j}\rangle = \exp(-i\theta)|1^{\gamma_i\gamma_j}\rangle$ , and  $G^{ij}(\theta)|0^{\gamma_i\gamma_j}\rangle = |0^{\gamma_i\gamma_j}\rangle$ . We will omit the upper indices when there is no confusion. Thus,  $R_{12} = \text{diag}(1, 1, G(\frac{\pi}{2}), G(\frac{\pi}{2}))$ , etc. On the other hand,  $R_{23}$  and  $R_{45}$  are naturally achieved by the delocalization of the two  $\chi$ MEMs at the edges of the two  $N = 1$   $\chi$ TSCs which are topologically protected (Fig. 5). The CNOT gate can therefore be achieved by a proper sequence of the  $R$ -matrices (Fig. 5b)

$$\text{CNOT} = R_{56}^{-1} R_{45} R_{34} R_{56} R_{45} R_{34}^{-1} R_{12} = \begin{pmatrix} 1 & 0 & 0 & 0 \\ 0 & 1 & 0 & 0 \\ 0 & 0 & 0 & 1 \\ 0 & 0 & 1 & 0 \end{pmatrix},$$

where  $R_{12}$  commutes with all other matrices. In designing the quantum gates, the operators associated with the propagation of the  $\chi$ MEMs are topological. Although the ones corresponding to the gate phase shift  $\theta$  are non-topological, the universal quantum computing based on the Ising type  $\chi$ MEMs is highly fault-tolerant [42, 43]. In other words, with the designed single-, double-qubits and the supplementary phase gates, universal quantum computing can be performed as long as the  $\chi$ MEMs are

coherent. The coherence of the  $\chi$ MEMs can be tested through the oscillation in the conductance  $\sigma_{23}$  between leads 2 and 3 in Fig. 5(a) by continuously tuning one of the phase gates between  $G_3$  and  $G_5$  while keeping all other gates stationary, similar to that in the Corbino structure discussed in Ref. [35].

In summary, we have shown that  $\chi$ TSCs can emerge from coupling the SC-TSS in superconductors with a topologically nontrivial band structure, such as in the Fe-based superconductor FeTeSe. The spin-triplet, inversion odd inter-surface pairing breaks time-reversal symmetry without magnetism and produces a 2D  $\chi$ TSC with a single  $\chi$ MEM at the boundary and MZM in the vortex core. The breaking of inversion symmetry under interchanges the two surfaces by gating or different substrates generally leads to mixing of singlet and triplet inter-surface pairing and increases the potential for realizing such intrinsic TSCs. Nonabelian braiding of the  $\chi$ MEMs and the detection of the half-integer quantized Hall conduc-

tance (see SI [31]) using the  $\chi$ TSC based devices can be more advantageous over the earlier proposal using the QAHI and SC proximity structures. Such devices can be fabricated using thin films of Fe-based superconductors with SC-TSS (Fig. 1a). We have proposed a novel CNOT gate device for universal quantum computing using such  $\chi$ TSC. A different double-surface structure is the opposing surfaces of two superconductors supporting the SC-TSS (Fig. 1b), e.g., the Josephson junction of two Fe-based superconductors. To explore the Majorana physics in such bilayer structures is a future task.

We thank Bin Chen, Dong-Lai Feng, Zheng-Cheng Gu, Kun Jiang, Jing Wang, Yi-Hua Wang, Yong-Shi Wu, and Sen Zhou for helpful discussions. This work is supported by NNSF of China with No. 11474061 (XL,YGC,YY), No. 11804223 (XL) and the U.S. Department of Energy, Basic Energy Sciences Grant No. DE-FG02-99ER45747 (ZW).

- 
- [1] A. Yu Kitaev, Fault-tolerant quantum computation by anyons, *Ann. Phys. (N.Y.)* **303**, (2003) 2.
- [2] S. Das Sarma, M. Freedman, C. Nayak, S. H. Simon, and A. Stern, Non-Abelian Anyons and Topological Quantum Computation, *Rev. Mod. Phys.* **80**, 1083 (2008).
- [3] G. Moore, and N. Read, Nonabelions in the fractional quantum Hall effect, *Nucl. Phys. B* **360**, 362 (1991).
- [4] N. Read, and D. Green, Paired states of fermions in two dimensions with breaking of parity and time-reversal symmetries and the fractional quantum Hall effect, *Phys. Rev. B* **61**, 10267 (2000).
- [5] For the recent experimental progresses, see, R. L. Willett, C. Nayak, K. Shtengel, L. N. Pfeiffer, and K. W. West, Magnetic field-tuned Aharonov-Bohm oscillations and evidence for non-Abelian anyons at  $\nu=5/2$ , *Phys. Rev. Lett.* **111**, 186401 (2013); R. L. Willett, K. Shtengel, C. Nayak, L.N. Pfeiffer, Y. J. Chung, M. L. Peabody, K. W. Baldwin, and K. W. West, Interference measurements of non-Abelian  $e/4$  and Abelian  $e/2$  quasiparticle braiding, arXiv:1905.10248.
- [6] X.-L. Qi, T. L. Hughes, and S.-C. Zhang, Chiral topological superconductor from the quantum Hall state, *Phys. Rev. B* **82**, 184516 (2010).
- [7] Qing Lin He, Lei Pan, Alexander L. Stern, Edward C. Burks, Xiaoyu Che., Gen Yin, Jing Wang, Biao Lian, Quan Zhou, Eun Sang Choi, Koichi Murata., Xufeng Kou, Zhijie Chen, Tianxiao Nie, Qiming Shao, Yabin Fan, Shou-Cheng Zhang, Kai Liu, Jing Xia, and Kang L. Wang, Chiral Majorana fermion modes in a quantum anomalous Hall insulator-superconductor structure, *Science* **357**, 294 (2017).
- [8] Morteza Kayyalha, Di Xiao, Ruoxi Zhang, Jaeho Shin, Jue Jiang, Fei Wang, Yi-Fan Zhao, Run Xiao, Ling Zhang, Kajetan M. Fijalkowski, Pankaj Mandal, Martin Winnerlein, Charles Gould, Qi Li, Laurens W. Molenkamp, Moses H. W. Chan, Nitin Samarth, and Cui-Zu Chang, Absence of evidence for chiral Majorana modes in quantum anomalous Hall-superconductor devices, *Science* **367**, 64 (2020).
- [9] Peng Zhang, Koichiro Yaji, Takahiro Hashimoto, Yuichi Ota, Takeshi Kondo, Kozo Okazaki, Zhijun Wang, Jinsheng Wen, G. D. Gu, Hong Ding, and Shik Shin, Observation of topological superconductivity on the surface of an iron-based superconductor *Science* **360**, 182 (2018).
- [10] S. Zhou, G. Kotliar, and Z. Wang, Superconductivity driven by charge fluctuations in iron-pnictides, *Phys. Rev. B* **84**, 140505(R) (2011).
- [11] Zhijun Wang, P. Zhang, Gang Xu, L. K. Zeng, H. Miao, Xiaoyan Xu, T. Qian, Hongming Weng, P. Richard, A. V. Fedorov, H. Ding, Xi Dai, and Zhong Fang, Topological Nature of the FeSe<sub>0.5</sub>Te<sub>0.5</sub> Superconductor, *Phys. Rev. B* **92**, 115119 (2015).
- [12] X. X. Wu, S. Qin, Y. Liang, H. Fan, and J. Hu, Topological Characters in FeTe<sub>1-x</sub>Se<sub>x</sub> Thin Films, *Phys. Rev. B* **93**, 115129 (2016).
- [13] G. Xu, B. Lian, P. Tang, X. L. Qi, and S. C. Zhang, Topological superconductivity on the surface of Fe-based superconductors, *Phys. Rev. Lett.* **117**, 047001 (2016).
- [14] Peng Zhang, Zhijun Wang, Xianxin Wu, Koichiro Yaji, Yukiaki Ishida, Yoshimitsu Kohama, Guangyang Dai, Yue Sun, Cedric Bareille, Kenta Kuroda, Takeshi Kondo, Kozo Okazaki, Koichi Kindo, Xiancheng Wang, Changqing Jin, Jiangping Hu, Ronny Thomale, Kazuki Sumida, Shilong Wu, Koji Miyamoto, Taichi Okuda, Hong Ding, G. D. Gu, Tsuyoshi Tamegai, Takuto Kawakami, Masatoshi Sato and Shik Shin, Multiple topological states in iron-based superconductors, *Nature Physics*, **15**, 41 (2019),
- [15] C. Caroli, P. G. de Gennes, and J. Matricon, Bound Fermion States on a Vortex Line in a Type II Superconductor, *Phys. Lett.* **9**, 307 (1964).
- [16] Kun Jiang, Xi Dai, and Ziqiang Wang, Quantum anomalous vortex and Majorana zero mode in iron-based superconductor Fe(Te,Se), *Phys. Rev. X* **9**, 011033 (2019).
- [17] L. Fu and C. L. Kane, Superconducting proximity effect and Majorana fermions at the surface of a topological insulator, *Phys. Rev. Lett.* **100**, 096407 (2008).
- [18] Dongfei Wang, Lingyuan Kong, Peng Fan, Hui Chen,

- Shiyu Zhu, Wenyao Liu, Lu Cao, Yujie Sun, Shixuan Du, John Schneeloch, Ruidan Zhong, Genda Gu, Liang Fu, Hong Ding, and Hong-Jun Gao, Evidence for Majorana bound state in an iron-based superconductor, *Science* **362**, 333 (2018).
- [19] T. Machida, Y. Sun, S. Pyon, S. Takeda, Y. Kohsaka, T. Hanaguri, T. Sasagawa, and T. Tamegai, Zero-energy vortex bound state in the superconducting topological surface state of Fe(Se,Te), *Nat. Mater.* **18**, 811 (2019).
- [20] Qin Liu, Chen Chen, Tong Zhang, Rui Peng, Ya-Jun Yan, Chen-Hao-Ping Wen, Xia Lou, Yu-Long Huang, Jin-Peng Tian, Xiao-Li Dong, Guang-Wei Wang, Wei-Cheng Bao, Qiang-Hua Wang, Zhi-Ping Yin, Zhong-Xian Zhao, and Dong-Lai Feng, Robust and clean Majorana zero mode in the vortex core of high-temperature superconductor ( $\text{Li}_{0.84}\text{Fe}_{0.16}$ )OHFeSe, *Phys. Rev. X* **8**, 041056(2018).
- [21] W. Liu, L. Cao, S. Zhu, L. Kong, G. Wang, M. Papaj, P. Zhang, Y. Liu, H. Chen, G. Li, F. Yang, T. Kondo, S. Du, G. Cao, S. Shin, L. Fu, Z. Yin, H.-J. Gao, and H. Ding, A new Majorana platform in an Fe-As bilayer superconductor, arXiv:1907.00904.
- [22] J-X. Yin, Zheng Wu, J-H. Wang, Z-Y. Ye, Jing Gong, X-Y. Hou, Lei Shan, Ang Li, X-J. Liang, X-X. Wu, Jian Li, C-S. Ting, Z-Q. Wang, J-P. Hu, P-H. Hor, H. Ding and S. H. Pan, Observation of a robust zero-energy bound state in iron-based superconductor Fe(Te,Se), *Nature Physics* **11**, 543(2015).
- [23] Peng Fan, Fazhi Yang, Guojian Qian, Hui Chen, Yuyang Zhang, Geng Li, Zihao Huang, Yuqing Xing, Lingyuan Kong, Wenyao Liu, Kun Jiang, Chengmin Shen, Shixuan Du, John Schneeloch, Ruidan Zhong, Genda Gu, Ziqiang Wang, Hong Ding, and Hong-Jun Gao, Reversible transition between Yu-Shiba-Rusinov state and Majorana zero mode by magnetic adatom manipulation in an iron-based superconductor, arXiv:2001.07376.
- [24] Songtian S. Zhang, Jia-Xin Yin, Guangyang Dai, Lingxiao Zhao, Tay-Rong Chang, Nana Shumiya, Kun Jiang, Hao Zheng, Guang Bian, Daniel Multer, Maksim Litskevich, Guoqing Chang, Ilya Belopolski, Tyler A. Cochran, Xianxin Wu, Desheng Wu, Jianlin Luo, Genfu Chen, Hsin Lin, Fang-Cheng Chou, Xiancheng Wang, Changqing Jin, Raman Sankar, Ziqiang Wang, and M. Zahid Hasan, Field-free platform for topological zero-energy mode in superconductors LiFeAs and PbTaSe<sub>2</sub>, arXiv:1912.11513.
- [25] L. Fu and E. Berg, Odd-Parity Topological Superconductors: Theory and Application to  $\text{Cu}_x\text{Bi}_2\text{Se}_3$ , *Phys. Rev. Lett.* **105**, 097001 (2010).
- [26] Corresponding matrices to Eq. (3) for complex pairing
- $$\begin{aligned} \text{Re}(h_{12}^{\Delta_s}) &= \sigma_0 \chi_y \tau_y, \quad \text{Im}(h_{12}^{\Delta_s}) = \sigma_0 \chi_y \tau_x, \\ \text{Re}(h_{12}^{\Delta_t}) &= \sigma_z \chi_x \tau_x, \quad \text{Im}(h_{12}^{\Delta_t}) = \sigma_z \chi_x \tau_y, \\ \text{Re}(h_{12}^{\Delta_{t\uparrow}} + h_{12}^{\Delta_{t\downarrow}}) &= \sigma_x \chi_x \tau_x, \quad \text{Re}(h_{12}^{\Delta_{t\uparrow}} - h_{12}^{\Delta_{t\downarrow}}) = \sigma_y \chi_x \tau_y, \\ \text{Im}(h_{12}^{\Delta_{t\uparrow}} + h_{12}^{\Delta_{t\downarrow}}) &= \sigma_x \chi_x \tau_y, \quad \text{Im}(h_{12}^{\Delta_{t\uparrow}} - h_{12}^{\Delta_{t\downarrow}}) = \sigma_y \chi_x \tau_x. \end{aligned}$$
- [27] L. Fu, Odd-parity topological superconductor with nematic order: Application to  $\text{Cu}_x\text{Bi}_2\text{Se}_3$ , *Phys. Rev. B* **90**, 100509(R)(2014).
- [28] A. P. Schnyder, S. Ryu, A. Furusaki, and A. W. W., Ludwig, Classification of topological insulators and superconductors in three spatial dimensions, *Phys. Rev. B* **78**, 195125 (2008).
- [29] S. Ryu, A. P. Schnyder, A. Furusaki, and A. W., W. Ludwig, Topological insulators and superconductors: tenfold way and dimensional hierarchy, *New J. Phys.* **12**, 065010 (2010).
- [30] A. Kitaev, Periodic table for topological insulators and superconductors, *AIP Conf. Proc.* **1134**, 22 (2009).
- [31] For more details, see Supplemental Information.
- [32] S. Rinott, K.B. Chashka A. Ribak, E. D. L. Rienks A. Taleb-Ibrahimi, P. Le Fevre, F. Bertran, M. Randeria, and A. Kanigel, Tuning across the BCS-BEC crossover in the multiband superconductor FeSeTe: An angle-resolved photoemission study, *Science Advances* **3**, e1602372 (2017).
- [33] D. J. Thouless, M. Kohmoto, M. P. Nightingale and M. den Nijs, Quantized Hall Conductance in a Two-Dimensional Periodic Potential, *Phys. Rev. Lett.* **49**, 405 (1982).
- [34] S. B. Chung, X.-L. Qi, J. Maciejko, and S.-C. Zhang, Conductance and noise signatures of Majorana backscattering, *Phys. Rev. B* **83**, 100512 (2011).
- [35] B. Lian, X.-Q. Sun, A. Vaezi, X.-L. Qi, and S.-C. Zhang, Topological quantum computation based on chiral Majorana fermions, *PNAS* **115**, 10938 (2018).
- [36] W. J. Ji, and X.-G. Wen,  $\frac{1}{2}(e^2/h)$  Conductance Plateau without 1D Chiral Majorana Fermions, *Phys. Rev. Lett.* **120**, 107002 (2018).
- [37] A. Stern and B. I. Halperin, Proposed Experiments to Probe the Non-Abelian  $\nu = 5/2$  Quantum Hall State, *Phys. Rev. Lett.* **96**, 016802 (2006).
- [38] P. Bonderson, A. Kitaev, and K. Shtengel, Detecting non-abelian statistics in the  $\nu=5/2$  fractional quantum Hall state, *Phys. Rev. Lett.* **96**, 016803 (2006).
- [39] C. Nayak and F. Wilczek, 2n-quasihole states realize  $2^{n-1}$ -dimensional spinor braiding statistics in paired quantum Hall states, *Nucl. Phys. B* **479**, 529 (1996).
- [40] D. A. Ivanov, Non-abelian statistics of Half-quantum vortices in p-wave superconductors, *Phys. Rev. Lett.* **86**, 268 (2001).
- [41] L. S. Georgiev, Topologically protected gates for quantum computation with non-Abelian anyons in the Pfaffian quantum Hall state, *Phys. Rev. B* **74**, 235112 (2006).
- [42] C. Nayak, S. H. Simon, A. Stern, M. Freedman, and S. Das Sarma, Non-abelian anyons and topological quantum computation, *Rev. Mod. Phys.* **80**, 1083 (2008).
- [43] L. S. Georgiev, Universal quantum computation with the  $\nu=5/2$  fractional quantum Hall state, *Phys. Rev. A* **73**, 042313 (2006).